BBA - Molecular Basis of Disease 1864 (2018) 3650–3658

Contents lists available at ScienceDirect

BBA - Molecular Basis of Disease

journal homepage: www.elsevier.com/locate/bbadis

# Barth syndrome cells display widespread remodeling of mitochondrial complexes without affecting metabolic flux distribution

Iliana A. Chatzispyrou[a], Sergio Guerrero-Castillo[b,1], Ntsiki M. Held[a,1], Jos P.N. Ruiter[a], Simone W. Denis[a], Lodewijk IJlst[a], Ronald J. Wanders[a], Michel van Weeghel[a], Sacha Ferdinandusse[a], Frédéric M. Vaz[a], Ulrich Brandt[b,*], Riekelt H. Houtkooper[a,**]

[a] Laboratory Genetic Metabolic Diseases, Amsterdam UMC, University of Amsterdam, Amsterdam Gastroenterology & Metabolism, Amsterdam Cardiovascular Sciences, Meibergdreef 9, 1105 AZ Amsterdam, the Netherlands

[b] Radboud Institute for Molecular Life Sciences, Department of Pediatrics, Radboud University Medical Center, Geert Grooteplein-Zuid 10, 6525 GA Nijmegen, the Netherlands.

ARTICLE INFO

*Keywords:*
Barth syndrome
Tafazzin
Mitochondria
Complexome profiling
Metabolomics
Respiratory chain Supercomplex
MICOS complex
2-Oxoglutarate dehydrogenase complex

ABSTRACT

Barth syndrome (BTHS) is a rare X-linked disorder that is characterized by cardiac and skeletal myopathy, neutropenia and growth abnormalities. The disease is caused by mutations in the *tafazzin* (*TAZ*) gene encoding an enzyme involved in the acyl chain remodeling of the mitochondrial phospholipid cardiolipin (CL). Biochemically, this leads to decreased levels of mature CL and accumulation of the intermediate monolysocardiolipin (MLCL). At a cellular level, this causes mitochondrial fragmentation and reduced stability of the respiratory chain supercomplexes. However, the exact mechanism through which *tafazzin* deficiency leads to disease development remains unclear. We therefore aimed to elucidate the pathways affected in BTHS cells by employing proteomic and metabolic profiling assays. Complexome profiling of patient skin fibroblasts revealed significant effects for about 200 different mitochondrial proteins. Prominently, we found a specific destabilization of higher order oxidative phosphorylation (OXPHOS) supercomplexes, as well as changes in complexes involved in cristae organization and CL trafficking. Moreover, the key metabolic complexes 2-oxoglutarate dehydrogenase (OGDH) and branched-chain ketoacid dehydrogenase (BCKD) were profoundly destabilized in BTHS patient samples. Surprisingly, metabolic flux distribution assays using stable isotope tracer-based metabolomics did not show reduced flux through the TCA cycle. Overall, insights from analyzing the impact of *TAZ* mutations on the mitochondrial complexome provided a better understanding of the resulting functional and structural consequences and thus the pathological mechanisms leading to Barth syndrome.

## 1. Introduction

Barth syndrome (BTHS) is a rare inherited X-linked disorder mainly characterized by cardiomyopathy, skeletal myopathy, neutropenia, 3-methylglutaconic aciduria and growth retardation with abnormal mitochondria [1–4]. BTHS is considered a multi-system disorder, as it presents with various additional symptoms that can differ between patients but also between different time points for the same patient [5]. When undiagnosed it can be fatal due to cardiac arrest or to bacterial sepsis during the early years of life [3]. The genetic cause of BTHS has been identified in the X-linked *tafazzin* (*TAZ*) gene, previously known as G4.5 [6,7], where pathogenic mutations spreading across all its 11 exons have been described [8]. The *TAZ* gene encodes the enzyme *tafazzin*, a mitochondrial acyltransferase involved in the remodeling of the phospholipid cardiolipin (CL) [9–11].

CL is considered the 'signature' phospholipid of mitochondria, as it is highly abundant in the organelle's membranes, comprising 10–15% of total lipid content particularly in the inner mitochondrial membrane

*Abbreviations:* BTHS, Barth syndrome; CL, cardiolipin; MLCL, monolysocardiolipin; OXPHOS, oxidative phosphorylation; TAZ, tafazzin

* Correspondence to: U. Brandt, Radboud Institute for Molecular Life Sciences, Department of Pediatrics, Radboud University Medical Center, Geert Grooteplein-Zuid 10, 6525 GA Nijmegen, the Netherlands.

** Correspondence to: R H. Houtkooper, Laboratory Genetic Metabolic Diseases, Amsterdam UMC, University of Amsterdam, Meibergdreef 9, 1105 AZ Amsterdam, the Netherlands.

*E-mail addresses:* ulrich.brandt@radboudumc.nl (U. Brandt), r.h.houtkooper@amc.uva.nl (R.H. Houtkooper).

[1] These authors have equally contributed to this work.

https://doi.org/10.1016/j.bbadis.2018.08.041
Received 3 May 2018; Received in revised form 25 July 2018; Accepted 30 August 2018
Available online 01 September 2018

[12]. Unlike other phospholipids that contain two fatty acyl chains, CL contains four, which gives it a conical structure and unique biophysical properties [13]. It is synthesized de novo in the inner mitochondrial membrane by the transfer of the phosphatidyl group of cytidinediphosphate-diacylglycerol to phosphatidylglycerol, which is catalyzed by CL synthase [11,14]. After its synthesis, the immature CL undergoes maturation, during which its initially saturated fatty acyl chains are remodeled to form a mature, more unsaturated CL [11]. The biosynthesis and remodeling of CL has been studied in depth in the yeast *Saccharomyces cerevisiae*, where newly synthesized CL is deacylated by the enzyme Cld1 which removes saturated fatty acyl chains from CL, forming the intermediate monolysocardiolipin (MLCL) with three fatty acyl chains [15]. Unsaturated fatty acyl chains are then transferred from phosphatidylcholine or phosphatidylethanolamine to MLCL by the yeast orthologue of *tafazzin*, Taz1, forming mature CL [16]. In mammals, remodeling of CL occurs in a similar fashion, with *tafazzin* serving the same function as described for yeast Taz1 [17].

BTHS patients with *TAZ* mutations present with a characteristic lipid profile of overall decreased CL levels, mainly of (poly)unsaturated species, and elevated levels of the remodeling intermediate MLCL [18–20]. This biochemical profile is highly specific for BTHS patients, and the MLCL/CL ratio is used as a diagnostic marker [21,22]. CL is crucial for mitochondrial membrane integrity and interacts with several mitochondrial proteins, including the multiprotein complexes of oxidative phosphorylation (OXPHOS) [9,13,23–26]. It is therefore not surprising that BTHS patients present with abnormal mitochondria in their tissues [1,27]. Also, *TAZ* mutations in several other model organisms including yeast, fruit fly, zebrafish and mouse, disrupt mitochondrial structure [28]. Despite the development of different models to study the pathophysiology of the disease, the exact underlying mechanism remains largely unresolved and treatment of patients is mainly symptomatic, while more targeted approaches are only recently being tested [3,29]. We therefore aimed to identify molecular pathways that are either dysregulated or activated in BTHS by employing proteomic and metabolic profiling in BTHS patient cells.

## 2. Materials and methods

### 2.1. Cell culture

Primary skin fibroblasts from four BTHS patients (P1: TAZ001, P2: TAZ002, P3: TAZ006 and P4: TAZ013) and three healthy controls C001, C127, C131) were obtained according to institutional guidelines and identifiable clinical and personal data from the patients were not available for this study. The BTHS patients and their CL/MLCL profiles were described before [30]. Cells were cultured in DMEM or Ham's F-10 with L-glutamine (Bio-Whittaker) growth media, supplemented with 10% fetal bovine serum (Bio-Whittaker), 25 mM HEPES buffer (Bio-Whittaker), 100 U/ml penicillin, 100 μg/ml streptomycin (Life Technologies), and 250 ng/ml Fungizone (Life Technologies) in a humidified atmosphere with 5% $CO_2$ at 37 °C.

### 2.2. Isolation of mitochondria

Isolation of mitochondria from skin fibroblasts was performed in principle as previously described [31]. Cell pellets were resuspended in 125 mM sucrose, 1 mM EDTA, 20 mM Tris/HCl pH 7.4 and disrupted by 10 strokes in a glass/Teflon Potter-Elvehjem homogenizer. The homogenates were mixed with 875 mM sucrose, 1 mM EDTA, 20 mM Tris/HCL pH 7.4 to adjust the sucrose concentration to 250 mM and centrifuged at 1000*g* for 10 min at 4 °C. Supernatants were centrifuged at 14000*g* for 10 min at 4 °C. The mitochondrial pellets were resuspended in 250 mM sucrose, 1 mM EDTA, 20 mM Tris/HCl pH 7.4. Protein concentration was determined by the Lowry method.

### 2.3. Complexome profiling

Mitochondrial pellets (200 μg protein) from a healthy control (C103) and four BTHS patient fibroblasts were solubilized with 6 mg digitonin/mg protein and separated by 4–16% gradient Blue-native PAGE (BN-PAGE) [32]. Complexome profiling was performed as before [33]. Protein identification and data analysis was done essentially as previously described [34] using MaxQuant (version 1.5.0.25) [35]. The profiles were hierarchically clustered by distance measures based on Pearson correlation coefficient (uncentered) and the average linkage method and further analyzed by manual correlation profiling. Mass scales of the profiles for soluble and integral membrane proteins were determined as previously described using known protein complexes as standards [33,34]. For comparison between the different samples, the total protein abundance (IBAQ) values were corrected for variations between the different profiles and then, the maximum abundance found in any of the profiles of the different samples was set to one for each individual protein. The clustering and the visualization and analysis of the heat maps were done with the NOVA software v0.5 [36] and MS Excel.

### 2.4. Metabolic flux measurement

100 U/ml penicillin, 100 μg/ml streptomycin (Life technologies), 25 mM HEPES (VWR) and 50 μM carnitine (Sigma) were added to DMEM without glucose, pyruvate, glutamine and phenol red to form the basal $^{13}C$ label medium. $^{13}C$-glucose labeling medium contained 5 mM [U$^{13}C$]-D-glucose (Cambridge Isotope Laboratories), 50 μM oleic acid in 0.2% BSA (Sigma) and 1 mM L-glutamine (Sigma). $^{13}C$-oleic acid labeling medium contained 50 μM [U$^{13}C$]-oleic acid in 2 g/l BSA (Cambridge Isotope Laboratories), 5 mM D-glucose (Sigma), and 1 mM L-glutamine (Sigma). Lastly, $^{13}C$-glutamine medium contained 1 mM [U$^{13}C$, 2-$^{15}$N]-glutamine (Cambridge Isotope Laboratories), 5 mM D-glucose (Sigma) and 50 μM oleic acid in 0.2% BSA (Sigma). 500.000 cells from 3 controls (C1: C001, C2: C127 and C3: C131) and 4 BTHS patients were plated per well in a 6-well plate. The next day 24 h incubations in any of the three $^{13}C$ media were initiated. For each condition, a duplicate incubation per labeled substrate was used. Polar metabolites were extracted by two-phase methanol-water/chloroform extraction as described in [37]. Briefly, medium was removed, cells were washed twice with ice-cold 0.9% (*w/v*) NaCl, 1 ml of ice-cold methanol-water (1:1) was added and cells were collected from the well in a centrifuge tube. 1 ml of chloroform was added to the mixture, tip sonicated and centrifuged at 10,000 x g for 10 min. Insoluble pellets were re-extracted with 1 ml methanol-water (1:1), the aqueous phase of both extractions was collected and evaporated using SpeedVac. The pellet was dissolved in 100 μl 60% (*v/v*) methanol/water and analyzed by ultra-high-pressure liquid chromatography system (Thermo Scientific) with a SeQuant ZIC-cHILIC column (Merck) coupled to a Thermo Q Exactive (Plus) Orbitrap mass spectrometer (Thermo Scientific). Data was acquired in negative ion-scan mode. Data interpretation was performed in Xcalibur software (Thermo Scientific). $^{13}C$-enrichment was calculated and corrected for their natural $^{13}C$ abundance based on mass isotopomer distribution analysis (MIDA) [38].

### 2.5. Enzyme activity measurements

OGDH-E1, OGDH-E3 and CS activities were measured in skin fibroblast homogenates from 3 healthy controls (C001, C123 and C124) and 4 BTHS patients. Cultured skin fibroblasts were harvested and stored at −80 °C until analysis. Before the analyses cell pellets were homogenized in 10 mM 4-morpholinopropanesulfonic acid (MOPS) pH 7.4, 160 mM sodium chloride and 0.1% Triton X-100. Cells were disrupted by sonication. E1 activity was measured spectrophotometrically at 340 nm using 2-oxoglutarate as substrate, as described in [39]. E3 activity was measured using an assay mixture

consisting of 50 mM potassium phosphate pH 6.5, 1.5 mM ethylenediaminetetraacetate (EDTA), 0.2 mM reduced nicotinamide adenine dinucleotide (NADH) and 0.15% *w/v* Triton X-100. Reactions were initiated by addition of lipoamide at a concentration of 2 mM dissolved in ethanol and the decrease in absorbance was followed in time at 340 nm. CS activity was measured using an assay mixture consisting of 100 mM TRIS pH 7.4, 0.1 mM DTNB (dithionitrobenzoic acid dissolved in 100 mM TRIS), 0.2 mM acetyl-CoA and 0.1% *w/v* Triton X-100. Reactions were initiated by addition of oxaloacetate at a concentration of 0.2 mM and the increase in absorbance was followed in time at 412 nm.

## 3. Results

### 3.1. Complexome analysis of human BTHS fibroblasts

To study whether there would be changes at the mitochondrial protein levels in BTHS patients' fibroblasts, we studied skin fibroblasts from four patients carrying different mutated versions of the *tafazzin* gene (P1: c.153C > G, P2: c.239-1G > A, P3: c.170G > T, P4: c.110-1G > C; [30]) and performed complexome profiling in comparison to a healthy control. This method [33] allows analyzing changes in the composition and abundance of mitochondrial complexes based on the migration profiles of their constituent proteins obtained by mass spectrometry after separation by blue native electrophoresis. Of 2769 proteins identified in total, 1238 were considered as mitochondrial based on different criteria. Initial manual inspection of the migration profiles for changes in abundance or shifts in molecular mass suggested possible effect of the TAZ mutations for about 200 mitochondrial proteins (Table S1). The most pronounced and remarkable differences will be discussed in the following.

The overall abundance of the five canonical OXPHOS complexes I–V was only mildly affected, if at all (Fig. 1). However, these complexes also associate into supercomplexes of variable composition [40]. In addition to the so-called respirasome containing complex I, one complex III dimer and up to four complex IV monomers (denoted $S_0$–$S_4$, where the number indicates the number of complex IV monomers), usually a small supercomplex containing one complex III dimer and one complex IV monomer ($III_2$-IV) is observed. Interestingly, we observed distinct changes in the relative distribution of the different variants of the respiratory chain supercomplexes (Fig. 1c). In mitochondrial membranes from cells of all four patients we observed partial destabilization of the supercomplexes, which was mirrored by the fact that the abundances of complex III dimer and the $III_2$-$IV_1$ supercomplex were increased. (Fig. 1b–c). Interestingly, especially the amounts of higher order respirasomes ($S_2$–$S_4$) were found to be markedly reduced in all patient samples (Fig. 1d).

It seems that apart from a mild overall destabilization of the respiratory supercomplexes, deficient CL remodeling affected in particular the interaction of complex IV with complexes I and III. For complex V, the major peak corresponding to monomeric $F_1F_O$ ATP-synthase seemed unaffected, but the amount of complex V dimer appeared markedly lower in all four patient samples (Fig. 1e). Complex II, which is not a component of respiratory chain supercomplexes, was clearly not affected (Fig. 1f).

Consistent with the reported aberrant mitochondrial morphology in BTHS [27,41], the TAZ mutations had also pronounced effects on proteins involved in cristae formation. A strong increase in abundance was observed for the mitochondrial contact site and cristae organizing system (MICOS) and the sorting and assembly machinery (SAM) complexes that together form the mitochondrial intermembrane space bridging complex (MIB) [34,42] (Fig. 2a). Of note, we observed a previously unresolved ~4 MDa version of the MIB complex. Similar to the MICOS/MIB complexes the dynamin-related GTPase OPA1, which binds lipid membranes enriched in CL and promotes membrane fusion [43], was markedly increased in abundance (Fig. 2b). Interestingly, a population of large OPA1 containing complexes broadly distributed from 0.5 to 5 MDa observed in control cells was missing in all four patient samples. In contrast to the overall increase of the MICOS/MIB components and OPA1, the total amount of LETM1, a mitochondrial proton/calcium antiporter reported to be involved in cristae organization and supercomplex assembly [41], was markedly reduced in patient cells (Fig. 2b). Moreover, while the majority of LETM1 was found at an apparent mass of ~150 kDa in the control samples, the majority of the remaining protein migrated below 100 kDa in samples from cells carrying TAZ mutations.

Furthermore, a several fold increase in abundance (Fig. 2c) was observed for the ~1 MDa prohibitin scaffolding complex and for the ~300 kDa the mitochondrial outer membrane pore complex consisting of the three isoforms of the voltage dependent anion channel protein VDAC (Fig. 2d).

All four TAZ mutations had a marked impact on the stability of the mitochondrial 2-oxoglutarate dehydrogenase complex (OGDH). In control cells, the three components E1-E3 of the complex comigrated in a sharp peak at an apparent molecular mass of ~4.4 MDa indicative of a homogenous population (Fig. 3a). Notably, prominent peaks of the dehydrogenase subunit E1 (OGDH) around 250 kDa and of dihydrolipoyldehydrogenase subunit E3 (DLD) around 350 kDa were also observed. In fact, the excess of DLD, which is a common component of all oxidative decarboxylases in mitochondria, was so high in this mass range that the DLD peak at ~4.4 MDa corresponding to the fraction of DLD bound to the OGDH complex appeared very small after normalization (Fig. 3a). KGD4, a protein also known as MRPS36 because it was originally annotated as a component of the mitochondrial ribosome, also comigrated with the full size OGDH complex. This corroborates a recent report showing that KGD4 is required in equimolar amounts to recruit DLD (E3) to the complex [44]. Strikingly, in mitochondria of all four patients the 4.4 MDa OGDH complex was not detectable. Instead, a rather broad and much smaller peak centered around 2.3 MDa appeared in the migration profiles of the core component DLST (E2) most likely reflecting a heterogeneous population of breakdown products of the OGDH-complex, which as well seemed to contain OGDH (E1) and to a lesser extent KGD4 (Fig. 3a). Reflecting the release of subunits from the full size OGDH complex in the patient samples, the amounts of the lower mass complexes of OGDH (E1) and DLD appeared higher and a small amount of a complex of KGD4 was now found around at ~250 kDa. Interestingly, the related branched-chain ketoacid dehydrogenase (BCKDH) complex was found to be affected in a similar way (Fig. 3b). Although the α- and β-subunits, which together constitute the E1 component of this enzyme, did not comigrate with a high molecular mass complex under the experimental conditions used, the majority of the lipoamide acyltransferase E2 component (DBT) was found as a sharp peak at ~3.6 MDa in the control sample. Like the OGDH complex, this 3.6 MDa complex was absent in all four patient samples and a heterogeneous population of smaller complexes at around 2 MDa was detected instead. Notably, a significant amount of the associated kinase BCKDK co-migrated with the 3.6 MDa DBT complex suggesting that a significant portion of this regulatory enzyme was bound to the core BCKDH complex, while its majority was found in a more heterogeneous population of complexes around 700 kDa. This notion was corroborated by the fact that the BCKDK peak disappeared in the patient samples as well.

### 3.2. Flux distribution analysis of human BTHS fibroblasts

We next questioned whether the observed changes in mitochondrial complexes of BTHS patient cells were reflected in the metabolism of these cells. To address this question, we performed metabolic flux distribution analysis on patient and control fibroblasts using $^{13}C$ isotope labelling and measuring labeled metabolites by mass spectrometry. In order to establish also whether the cells demonstrated a preference for a specific energy source, we used three different $^{13}C$-labeled substrates, namely glucose, oleic acid and glutamine. To evaluate substrate

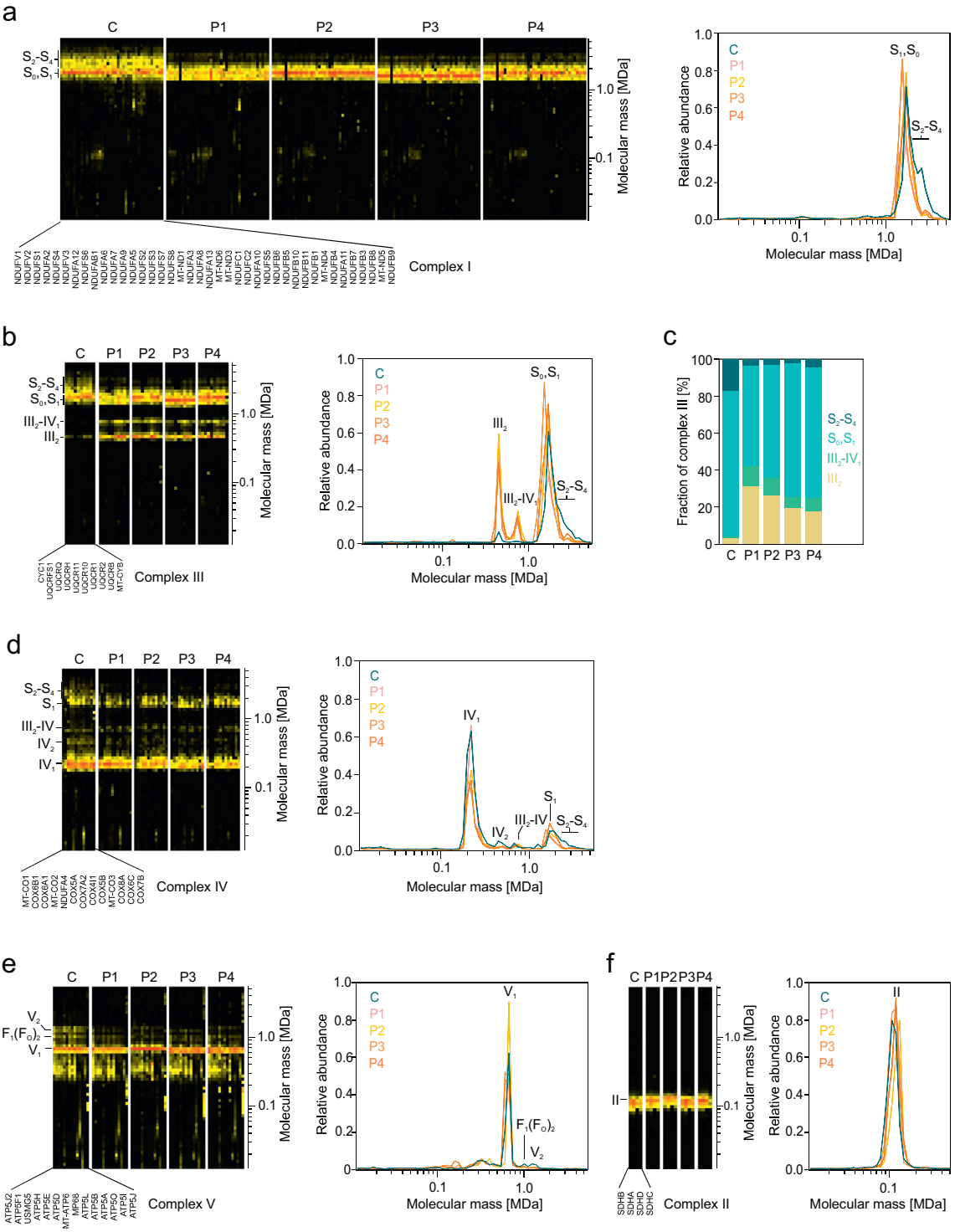


**Fig. 1.** *Higher order OXPHOS supercomplexes are destabilized in skin fibroblasts of BTHS patients.* a, complex I; b, complex III; c, relative distribution of supercomplexes calculated from the relative abundance of complex III, which is assumed to have the same stoichiometry in all supercomplexes; d, complex IV; e, complex V; f, complex II. In panels a-b and d-f the migration profiles are shown on the left as heat map representations indicating increasing relative protein abundance by a color code from yellow to red and plotting the migration patterns of the individual subunits from top to bottom. On the right normalized relative abundance plots show the average migration profiles of all subunits detected for the respective OXPHOS complex. OXPHOS complexes are indicated by roman numerals and supercomplexes by the S. Subscripts indicate the copy number of the respective complex and of complex IV for supercomplexes. $F_1$,$F_O$, $F_1$, $F_O$ moiety of complex V; C, control; P1–4, samples from patients 1–4.

preference, we performed separate incubations for each of the $^{13}$C-labeled substrates, i.e. every incubation contained the same glucose, oleic acid and glutamine concentrations but only one of the three substrates was labeled.

After 24 h of incubation with the different labeled substrates, we determined $^{13}$C incorporation in different TCA cycle intermediates as a measure of substrate utilization and TCA cycle activity in the cells. Glucose carbon incorporation in TCA cycle intermediates was overall low in both patients and controls (< 10%; Table S2), while incorporation into glycolysis intermediates and end products such as

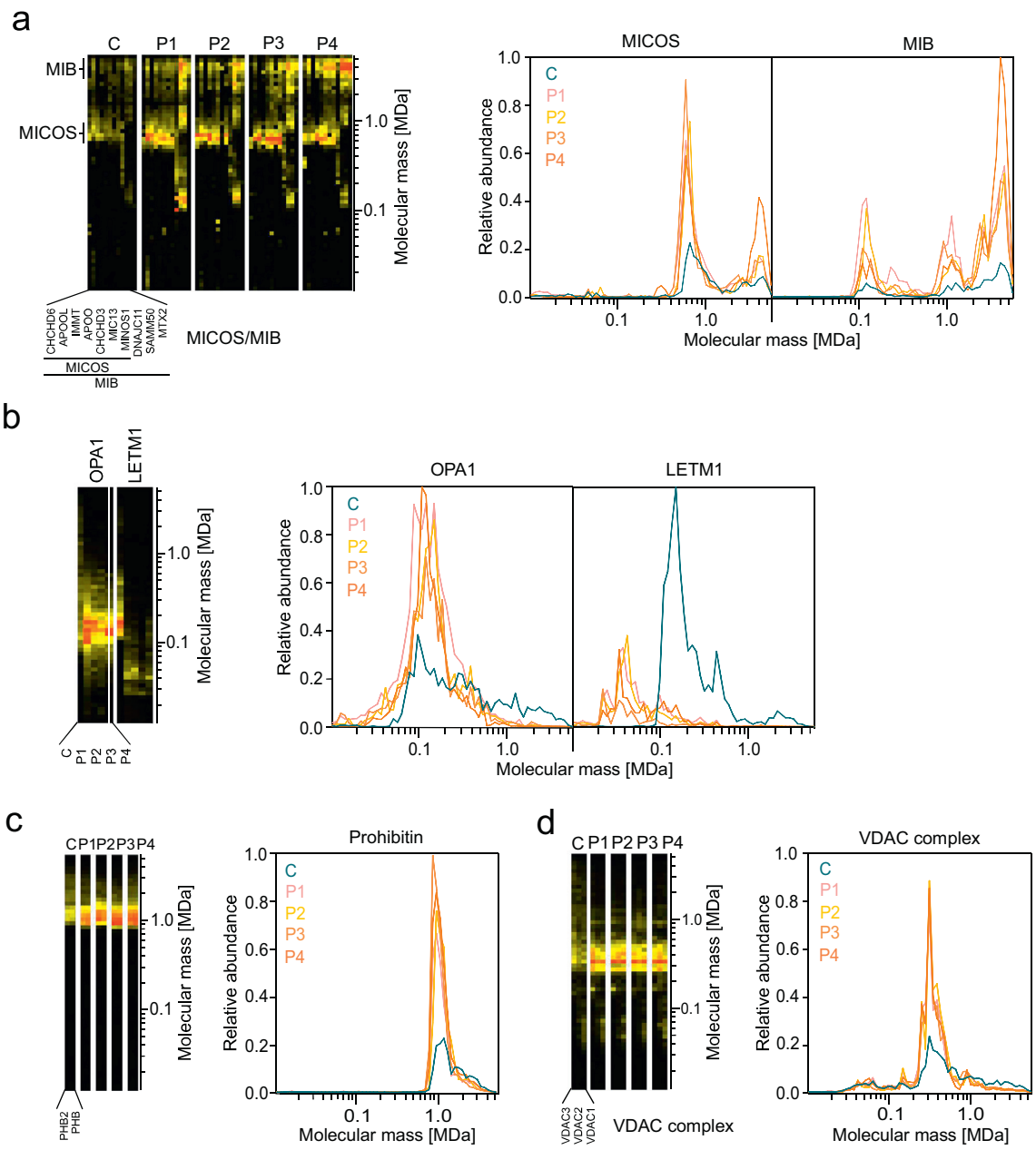


**Fig. 2.** *The abundance of protein complexes of the outer and inner mitochondrial membranes is markedly changed in skin fibroblasts of BTHS patients.* a, mitochondrial contact site and cristae organizing system (MICOS) and mitochondrial intermembrane space bridging complex (MIB) complex; b, dynamin-related GTPase OPA1 and mitochondrial proton/calcium antiporter LETM1; c, prohibitin (PHB) scaffolding complex of the inner mitochondrial membrane; d, voltage dependent anion channel (VDAC) complex of the outer mitochondrial membrane. See legend of Fig. 1 for details. In panel b abundance plots of individual components are shown.

lactate was similar between controls and patients (Table S3). When comparing label incorporation from the three substrates, glutamine appeared the most successful, since > 65% of the 2-oxoglutarate pool was labeled by glutamine in both control and patient groups through glutaminolysis (Fig. 4; Table S4). We did not find a significant reduction in glutamine-derived carbon label in any of the downstream TCA cycle intermediates (Fig. 4; Table S4). This suggested that BTHS cells are able to sustain sufficient OGDH flux despite the impaired stability of the OGDH complex. Furthermore, when $^{13}$C-oleic acid was added as a substrate, labeling was highest in citrate but very low in downstream metabolites (Fig. 4; Table S5). Oleic acid carbons enter the TCA cycle via acetyl-CoA, therefore, the first TCA cycle intermediate to be labeled is citrate. Labeling of downstream TCA cycle intermediates was much lower in both controls and patients, probably because the unlabeled glutamine was used by these cells via glutaminolysis as the prime substrate.

### 3.3. TCA cycle enzymatic assays in BTHS human fibroblasts

BTHS patient cells exhibited a reduced OGDH stability while maintaining sufficient metabolic flux through this enzyme complex. To assess whether the complex destabilization led to a defect at the level of the isolated OGDH enzyme, we set out to directly measure the 2-oxoglutarate dehydrogenase activity conferred by the E1 component of the OGDH complex in cell homogenates. We also measured the activity of dihydrolipoamide dehydrogenase (DLD), also known as E3, which is a common subunit of all enzyme complexes catalyzing oxidative decarboxylation of 2-oxoacids and is also a component of the BCKDH complex that was found to be destabilized in BTHS patients as well (Fig. 3b). As a reference, we measured the activity of another enzyme of

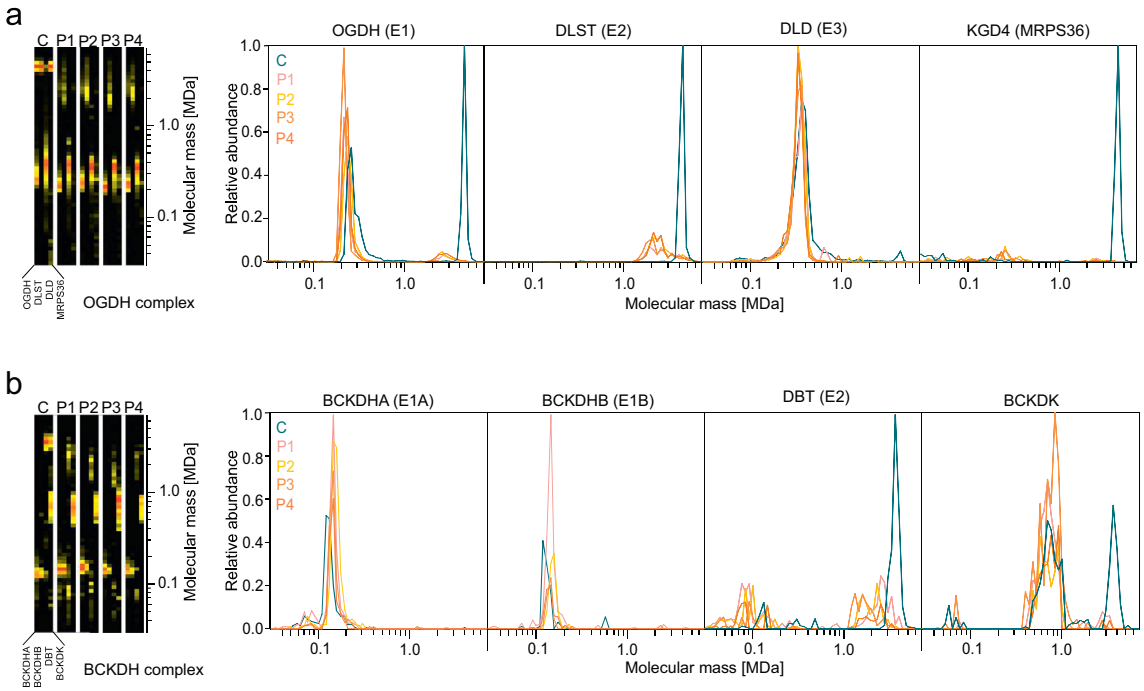


**Fig. 3.** *Key metabolic complexes are destabilized in skin fibroblasts of BTHS patients.* a, 2-Oxoglutarate-dehydrogenase (OGDH complex); b, branched chain ketoacid dehydrogenase (BCKDH) complex. See legend of Fig. 1 and text for further details.

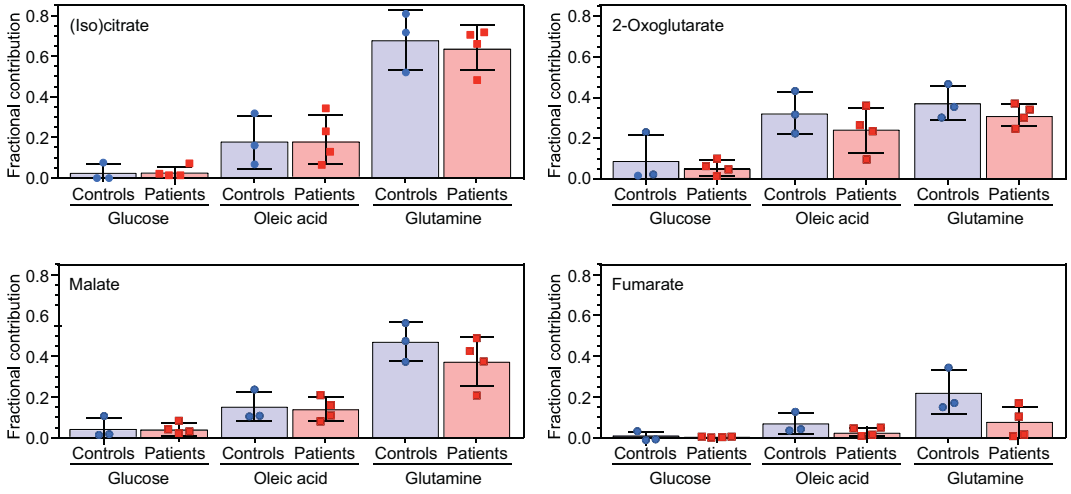


**Fig. 4.** *Metabolic flux distribution is unaffected in BTHS skin fibroblasts.* Bar graphs depict the fractional contribution into four TCA metabolites (citrate, 2-oxoglutarate, malate and fumarate) after 24 h incubation with medium containing $^{13}C$ labeled glucose, oleic acid or glutamine. The substrate concentration was the same in all incubation media. Controls (blue) and samples from patients 1–4 (red) were measured as technical duplicates. Data are given as the mean ± SD and statistical significance was calculated by a student's *t*-test.

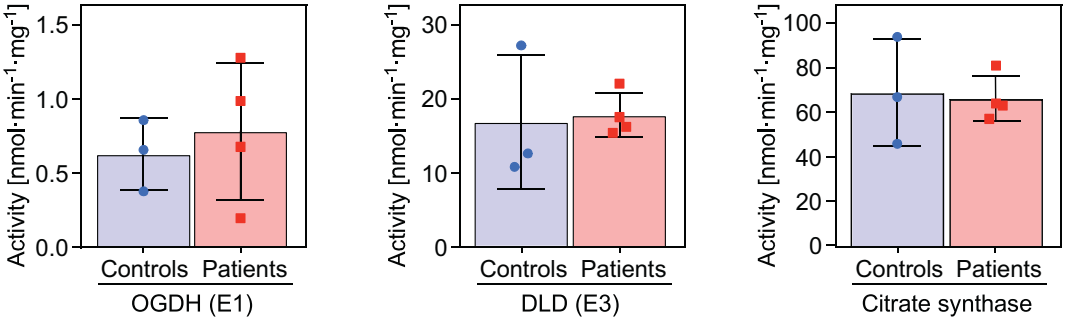


**Fig. 5.** *Enzyme activities of E1 and E3 of oxidative decarboxylation complexes are not affected in BTHS fibroblasts.* Controls (blue) and samples from patients 1–4 (red) were measured as technical duplicates. Data are given as the mean ± SD.

the mitochondrial matrix, citrate synthase (CS). The activities of all three enzymes varied substantially even within the controls and patient samples and thus differences could not be attributed to the TAZ mutations (Fig. 5).

## 4. Discussion

Defective CL remodeling in BTHS has been shown to affect mitochondria in different ways ranging from the destabilization of various multiprotein complexes [25,26,45,46] to aberrant cristae morphology [27,41]. However, it remains largely unclear, how the observed changes in the molecular architecture lead to functional consequences like altered production of reactive oxygen species [28] and inhibition of apoptosis [45] that ultimately result in the BTHS disease phenotype. Therefore, we aimed to obtain a more detailed understanding of the molecular mechanisms underlying BTHS by comprehensively assessing the changes resulting from mutations in the TAZ gene at the level of the mitochondrial complexome and by linking the observed alterations to metabolic flux distribution in BTHS patient cells. Complexome analysis of mitochondria of fibroblasts from patients carrying four different mutations in the TAZ gene revealed changes in a remarkably large number of proteins covering a wide range of functions (Table S1). Here we focus on analyzing the most prominently affected protein complexes.

CL is long known to be required for the stability of the OXPHOS supercomplexes [47] and it has been shown previously that deficient CL biosynthesis and remodeling can destabilize them [26,45,48]. The complexome profiling analysis of BTHS fibroblasts presented here corroborated these findings and revealed that defective CL remodeling specifically destabilized higher order OXPHOS supercomplexes containing multiple copies of complex IV (Fig. 1a-d). Notably, interaction between complexes III and IV appeared not to be affected. Since complex IV has been shown to interact with complexes I and III in mammalian supercomplexes [49] this suggested that the altered CL species composition primarily impairs the complex I-IV interaction. Recently, several structures of mitochondrial respiratory chain supercomplexes were obtained, but all of them contain only one complex IV monomer per complex I [50–52]. Several cardiolipin molecules were modeled into these structures, some of which may be involved in the interactions between the complexes. However, at the moderate structural resolution achieved in these studies, if any, only some of the lipids bound to a membrane protein complex can be found and the assignment of specific fatty acids to the bound cardiolipins is not possible. Thus, the structural information presently available is not sufficient to analyse the interaction between complex IV and the other complexes in molecular detail. This holds especially for the binding of the additional complex IV moieties in supercomplexes $S_{2–4}$, which were found to be most affected in our present study.

Another higher order assembly affected by the TAZ mutations were the dimers of complex V, which were clearly destabilized in the patient samples (Fig. 1e). Since rows of ATPase dimers are known to shape curved inner mitochondrial membranes [53], their destabilization could contribute to the altered cristae morphology in BTHS [27,41]. This notion corresponds well with a several fold overall increase in abundance of the MICOS/MIB complexes (Fig. 2a), which are key players in the organization of the inner mitochondrial membrane and the formation of contact sites with the outer membrane [34,54]. Moreover, strongly increased amounts of the mitochondrial fusion and cristae regulator OPA1 were detected in BTHS patient cells (Fig. 2b). On the other hand, a ~150 kDa complex of LETM1, another factor known to be involved in mitochondrial morphogenesis, was absent in cells carrying TAZ mutations and the total abundance of this protein was markedly reduced (Fig. 2b). Based on these findings it is tempting to speculate that the destabilization of OXPHOS complexes and in particular complex V dimers by the aberrant CL, impairs normal cristae formation in BTHS mitochondria and results in upregulation of the MICOS/MIB complexes and other compensatory adaptations of the machinery controlling mitochondrial morphology.

Two more membrane protein complexes known to interact with CL exhibited a several-fold higher abundance in BTHS patient cells, namely the inner membrane scaffolding complex prohibitin (Fig. 2c), which has been implicated in CL remodeling [55], and the outer membrane VDAC complex (Fig. 2d), which has been reported to polymerize in a CL dependent fashion [56]. Of note and in contrast to our findings, downregulation of prohibitin was found in the yeast *Saccharomyces cerevisiae* upon deletion of the TAZ gene [46].

Remarkably, we observed the most dramatic effect of impaired CL remodeling in BTHS patient cells for two soluble multienzyme complexes of the family of oxidative decarboxylases. The large multiprotein complexes of 2-oxoglutarate dehydrogenase (OGDH), a TCA cycle enzyme, and branched-chain ketoacid dehydrogenase (BCKDH), involved in the degradation of branched chain amino acids, were easily detectable in control cells but were completely absent in the patient samples (Fig. 3). This finding is in line with an earlier report showing that deletion of the TAZ gene in yeast results in a marked decrease of fully assembled OGDH complex [46]. Further inspection of the complexome profiles revealed that, while the ~4.4 MDa OGDH complex contained all four known components (E1-E3 and KGD4), the two proteins forming the E1 component were found to be stripped off from the ~3.6 BCKDH holo-complex even in the control sample. Instead, the regulatory kinase BCKDK comigrated with the E2 component of the BCKDH complex suggesting that a significant fraction of this protein was tightly bound to the E2 core complex. Smaller assemblies of all subunits of the oxidative decarboxylation complexes were detected also in the patient samples. However, while the total amount of the E2 component and KDG4 was markedly lower, the overall abundance of E1, E3 and BCKDK appeared essentially unchanged. Indeed, we found that the catalytic activities of the E1 and E3 components of the OGDH complex at substrate saturation were not affected by the TAZ mutations (Fig. 5).

While the molecular cause for the observed drastic destabilization of the full size OGDH and BCKDH complexes by impaired CL remodeling remained obscure, we went on to establish its metabolic effects. To this end, we measured metabolic flux distribution using three different substrates. Glucose appeared to contribute minimally to the TCA flux, as the incorporation into TCA cycle intermediates was low. Glutamine directly feeds into the TCA cycle and, consequently, $^{13}C$ incorporation was high compared the other substrates suggesting high glutamine utilization. When using labeled oleic acid, only a slight trend for reduced labeling of citrate was observed, while the downstream TCA cycle metabolites were clearly not affected. Given that glutaminolysis was very active under the conditions used, unlabeled glutamine probably diluted the $^{13}C$ label from oleic acid in downstream TCA intermediates thereby completely masking the mild effect, which even for citrate did not reach statistical significance. When using glutamine as a labeled substrate we observed no difference in flux distribution at the level of TCA cycle intermediates. This is rather surprising considering that the full-size complex was not at all detectable in the patient samples. We conclude that the TAZ mutations do not completely prevent the assembly of functional OGDH complex, but that the destabilization of the full-size complex evident from its complete dissociation under the conditions of complexome profiling merely resulted in partially reduced levels of functional OGDH complex in-situ, explaining the observed moderate effects on glutamine dependent metabolic flux. Moreover, it seems quite possible that the observed destabilization of the OGDH complex, despite having only minor functional consequence in fibroblasts, may have significant relevant functional impact in tissues that are in high energy demand.

In conclusion, using complexome profiling of BTHS patient cells, we obtained a comprehensive assessment of the consequences of impaired CL remodeling on the state, distribution and abundance of a number of key mitochondrial multiprotein complexes. These findings could be

correlated with structural and metabolic adaptations in BTHS and provided novel insights into the molecular details of supercomplex destabilization, aberrant cristae morphology and metabolic changes resulting from TAZ mutations. Moreover, the complexome data presented here will be a valuable resource for further studies of BTHS induced changes at the level of proteins and protein complexes, which could not be analyzed further within the scope of the present study.

Supplementary data to this article can be found online at https://doi.org/10.1016/j.bbadis.2018.08.041.

## Transparency document

The Transparency document associated with this article can be found, in online version.

## Acknowledgements

We thank Martijn Huynen for helpful discussions. I.A.C. is supported by a PhD Scholarship from the Academic Medical Center of Amsterdam. Work in the Houtkooper group is financially supported by a VIDI grant from the Netherlands Organization for Health Research and Development (no. 91715305). U.B. was supported by grant BR 1633/3-1 within SPP1710 of the Deutsche Forschungsgemeinschaft and a TOP grant from the Netherlands Organization for Health Research and Development (no. 91217009).

## References

[1] P.G. Barth, H.R. Scholte, J.A. Berden, J.M. Van der Klei-Van Moorsel, I.E. Luyt-Houwen, E.T. Van't veVer Korthof, J.J. Van der Harten, M.A. Sobotka-Plojhar, An X-linked mitochondrial disease affecting cardiac muscle, skeletal muscle and neutrophil leucocytes, J. Neurol. Sci. 62 (1983) 327–355.
[2] H.B. Neustein, P.R. Lurie, B. Dahms, M. Takahashi, An X-linked recessive cardiomyopathy with abnormal mitochondria, Pediatrics 64 (1979) 24–29.
[3] S.L. Clarke, A. Bowron, I.L. Gonzalez, S.J. Groves, R. Newbury-Ecob, N. Clayton, R.P. Martin, B. Tsai-Goodman, V. Garratt, M. Ashworth, V.M. Bowen, K.R. McCurdy, M.K. Damin, C.T. Spencer, M.J. Toth, R.I. Kelley, C.G. Steward, Barth syndrome, Orphanet J Rare Dis 8 (2013) 23.
[4] R.I. Kelley, J.P. Cheatham, B.J. Clark, M.A. Nigro, B.R. Powell, G.W. Sherwood, J.T. Sladky, W.P. Swisher, X-linked dilated cardiomyopathy with neutropenia, growth retardation, and 3-methylglutaconic aciduria, J. Pediatr. 119 (1991) 738–747.
[5] A.E. Roberts, C. Nixon, C.G. Steward, K. Gauvreau, M. Maisenbacher, M. Fletcher, J. Geva, B.J. Byrne, C.T. Spencer, The Barth syndrome registry: distinguishing disease characteristics and growth data from a longitudinal study, Am. J. Med. Genet. A 158A (2012) 2726–2732.
[6] S. Bione, P. D'Adamo, E. Maestrini, A.K. Gedeon, P.A. Bolhuis, D. Toniolo, A novel X-linked gene, G4.5. Is responsible for Barth syndrome, Nat. Genet. 12 (1996) 385–389.
[7] J. Johnston, R.I. Kelley, A. Feigenbaum, G.F. Cox, G.S. Iyer, V.L. Funanage, R. Proujansky, Mutation characterization and genotype-phenotype correlation in Barth syndrome, Am. J. Hum. Genet. 61 (1997) 1053–1058.
[8] I.L. Gonzalez, Barth syndrome: TAZ gene mutations, mRNAs, and evolution, Am. J. Med. Genet. A 134 (2005) 409–414.
[9] R.H. Houtkooper, F.M. Vaz, Cardiolipin, the heart of mitochondrial metabolism, Cell. Mol. Life Sci. 65 (2008) 2493–2506.
[10] F.M. Vaz, R.H. Houtkooper, F. Valianpour, P.G. Barth, R.J. Wanders, Only one splice variant of the human TAZ gene encodes a functional protein with a role in cardiolipin metabolism, J. Biol. Chem. 278 (2003) 43089–43094.
[11] G.J. Gaspard, C.R. McMaster, Cardiolipin metabolism and its causal role in the etiology of the inherited cardiomyopathy Barth syndrome, Chem. Phys. Lipids 193 (2015) 1–10.
[12] S.E. Horvath, G. Daum, Lipids of mitochondria, Prog. Lipid Res. 52 (2013) 590–614.
[13] M. Schlame, D. Rua, M.L. Greenberg, The biosynthesis and functional role of cardiolipin, Prog. Lipid Res. 39 (2000) 257–288.
[14] R.H. Houtkooper, H. Akbari, H. van Lenthe, W. Kulik, R.J. Wanders, M. Frentzen, F.M. Vaz, Identification and characterization of human cardiolipin synthase, FEBS Lett. 580 (2006) 3059–3064.
[15] A. Beranek, G. Rechberger, H. Knauer, H. Wolinski, S.D. Kohlwein, R. Leber, Identification of a cardiolipin-specific phospholipase encoded by the gene CLD1 (YGR110W) in yeast, J. Biol. Chem. 284 (2009) 11572–11578.
[16] Z. Gu, F. Valianpour, S. Chen, F.M. Vaz, G.A. Hakkaart, R.J. Wanders, M.L. Greenberg, Aberrant cardiolipin metabolism in the yeast taz1 mutant: a model for Barth syndrome, Mol. Microbiol. 51 (2004) 149–158.
[17] Y. Xu, S. Zhang, A. Malhotra, I. Edelman-Novemsky, J. Ma, A. Kruppa, C. Cernicica, S. Blais, T.A. Neubert, M. Ren, M. Schlame, Characterization of tafazzin splice variants from humans and fruit flies, J. Biol. Chem. 284 (2009) 29230–29239.
[18] P. Vreken, F. Valianpour, L.G. Nijtmans, L.A. Grivell, B. Plecko, R.J. Wanders, P.G. Barth, Defective remodeling of cardiolipin and phosphatidylglycerol in Barth syndrome, Biochem. Biophys. Res. Commun. 279 (2000) 378–382.
[19] M.A. van Werkhoven, D.R. Thorburn, A.K. Gedeon, J.J. Pitt, Monolysocardiolipin in cultured fibroblasts is a sensitive and specific marker for Barth syndrome, J. Lipid Res. 47 (2006) 2346–2351.
[20] M. Schlame, J.A. Towbin, P.M. Heerdt, R. Jehle, S. Dimauro, T.J. Blanck, Deficiency of tetralinoleoyl-cardiolipin in Barth syndrome, Ann. Neurol. 51 (2002) 634–637.
[21] W. Kulik, H. van Lenthe, F.S. Stet, R.H. Houtkooper, H. Kemp, J.E. Stone, C.G. Steward, R.J. Wanders, F.M. Vaz, Bloodspot assay using HPLC-tandem mass spectrometry for detection of Barth syndrome, Clin. Chem. 54 (2008) 371–378.
[22] R.H. Houtkooper, R.J. Rodenburg, C. Thiels, H. van Lenthe, F. Stet, B.T. Poll-The, J.E. Stone, C.G. Steward, R.J. Wanders, J. Smeitink, W. Kulik, F.M. Vaz, Cardiolipin and monolysocardiolipin analysis in fibroblasts, lymphocytes, and tissues using high-performance liquid chromatography-mass spectrometry as a diagnostic test for Barth syndrome, Anal. Biochem. 387 (2009) 230–237.
[23] V. Koshkin, M.L. Greenberg, Cardiolipin prevents rate-dependent uncoupling and provides osmotic stability in yeast mitochondria, Biochem. J. 364 (2002) 317–322.
[24] M. Klingenberg, Cardiolipin and mitochondrial carriers, Biochim. Biophys. Acta 1788 (2009) 2048–2058.
[25] K. Brandner, D.U. Mick, A.E. Frazier, R.D. Taylor, C. Meisinger, P. Rehling, Taz1, an outer mitochondrial membrane protein, affects stability and assembly of inner membrane protein complexes: implications for Barth syndrome, Mol. Biol. Cell 16 (2005) 5202–5214.
[26] M. McKenzie, M. Lazarou, D.R. Thorburn, M.T. Ryan, Mitochondrial respiratory chain supercomplexes are destabilized in Barth syndrome patients, J. Mol. Biol. 361 (2006) 462–469.
[27] D. Acehan, Y. Xu, D.L. Stokes, M. Schlame, Comparison of lymphoblast mitochondria from normal subjects and patients with Barth syndrome using electron microscopic tomography, Lab. Investig. 87 (2007) 40–48.
[28] A. Saric, K. Andreau, A.S. Armand, I.M. Moller, P.X. Petit, Barth syndrome: from mitochondrial dysfunctions associated with aberrant production of reactive oxygen species to pluripotent stem cell studies, Front. Genet. 6 (2015) 359.
[29] A. Malhotra, P. Kahlon, T. Donoho, I.C. Doyle, Pharmacogenomic considerations in the treatment of the pediatric cardiomyopathy called Barth syndrome, Recent Pat Biotechnol 8 (2014) 136–143.
[30] R.H. Houtkooper, M. Turkenburg, B.T. Poll-The, D. Karall, C. Perez-Cerda, A. Morrone, S. Malvagia, R.J. Wanders, W. Kulik, F.M. Vaz, The enigmatic role of tafazzin in cardiolipin metabolism, Biochim. Biophys. Acta 1788 (2009) 2003–2014.
[31] A.J. Janssen, F.J. Trijbels, R.C. Sengers, J.A. Smeitink, L.P. van den Heuvel, L.T. Wintjes, B.J. Stoltenborg-Hogenkamp, R.J. Rodenburg, Spectrophotometric assay for complex I of the respiratory chain in tissue samples and cultured fibroblasts, Clin. Chem. 53 (2007) 729–734.
[32] I. Wittig, H.P. Braun, H. Schägger, Blue native PAGE, Nat. Protoc. 1 (2006) 418–428.
[33] H. Heide, L. Bleier, M. Steger, J. Ackermann, S. Drose, B. Schwamb, M. Zornig, A.S. Reichert, I. Koch, I. Wittig, U. Brandt, Complexome profiling identifies TMEM126B as a component of the mitochondrial complex I assembly complex, Cell Metab. 16 (2012) 538–549.
[34] M.A. Huynen, M. Muhlmeister, K. Gotthardt, S. Guerrero-Castillo, U. Brandt, Evolution and structural organization of the mitochondrial contact site (MICOS) complex and the mitochondrial intermembrane space bridging (MIB) complex, Biochim. Biophys. Acta 1863 (2016) 91–101.
[35] J. Cox, M. Mann, MaxQuant enables high peptide identification rates, individualized p.P.B.-range mass accuracies and proteome-wide protein quantification, Nat. Biotechnol. 26 (2008) 1367–1372.
[36] H. Giese, J. Ackermann, H. Heide, L. Bleier, S. Drose, I. Wittig, U. Brandt, I. Koch, NOVA: a software to analyze complexome profiling data, Bioinformatics 31 (2015) 440–441.
[37] S.C. Sapcariu, T. Kanashova, D. Weindl, J. Ghelfi, G. Dittmar, K. Hiller, Simultaneous extraction of proteins and metabolites from cells in culture, MethodsX 1 (2014) 74–80.
[38] M. Fernandez-Fernandez, P. Rodriguez-Gonzalez, J.I. Garcia Alonso, A simplified calculation procedure for mass isotopomer distribution analysis (MIDA) based on multiple linear regression, J. Mass Spectrom. 51 (2016) 980–987.
[39] R.J. Dunckelmann, F. Ebinger, A. Schulze, R.J. Wanders, D. Rating, E. Mayatepek, 2-Ketoglutarate dehydrogenase deficiency with intermittent 2-ketoglutaric aciduria, Neuropediatrics 31 (2000) 35–38.
[40] H. Schägger, K. Pfeiffer, Supercomplexes in the respiratory chains of yeast and mammalian mitochondria, EMBO J. 19 (2000) 1777–1783.
[41] S. Tamai, H. Iida, S. Yokota, T. Sayano, S. Kiguchiya, N. Ishihara, J. Hayashi, K. Mihara, T. Oka, Characterization of the mitochondrial protein LETM1, which maintains the mitochondrial tubular shapes and interacts with the AAA-ATPase BCS1L, J. Cell Sci. 121 (2008) 2588–2600.
[42] V. Kozjak-Pavlovic, The MICOS complex of human mitochondria, Cell Tissue Res. 367 (2017) 83–93.
[43] T. Ban, J.A. Heymann, Z. Song, J.E. Hinshaw, D.C. Chan, OPA1 disease alleles causing dominant optic atrophy have defects in cardiolipin-stimulated GTP hydrolysis and membrane tubulation, Hum. Mol. Genet. 19 (2010) 2113–2122.
[44] M. Heublein, M.A. Burguillos, F.N. Vogtle, P.F. Teixeira, A. Imhof, C. Meisinger, M. Ott, The novel component Kgd4 recruits the E3 subunit to the mitochondrial alpha-ketoglutarate dehydrogenase, Mol. Biol. Cell 25 (2014) 3342–3349.
[45] F. Gonzalvez, M. D'Aurelio, M. Boutant, A. Moustapha, J.P. Puech, T. Landes, L. Arnaune-Pelloquin, G. Vial, N. Taleux, C. Slomianny, R.J. Wanders, R.H. Houtkooper, P. Bellenguer, I.M. Moller, E. Gottlieb, F.M. Vaz, G. Manfredi,

P.X. Petit, Barth syndrome: cellular compensation of mitochondrial dysfunction and apoptosis inhibition due to changes in cardiolipin remodeling linked to tafazzin (TAZ) gene mutation, Biochim. Biophys. Acta 1832 (2013) 1194–1206.
[46] R.A. van Gestel, P.J. Rijken, S. Surinova, M. O'Flaherty, A.J. Heck, J.A. Killian, A.I. de Kroon, M. Slijper, The influence of the acyl chain composition of cardiolipin on the stability of mitochondrial complexes; an unexpected effect of cardiolipin in alpha-ketoglutarate dehydrogenase and prohibitin complexes, J. Proteome 73 (2010) 806–814.
[47] K. Pfeiffer, V. Gohil, R.A. Stuart, C. Hunte, U. Brandt, M.L. Greenberg, H. Schägger, Cardiolipin stabilizes respiratory chain supercomplexes, J. Biol. Chem. 278 (2003) 52873–52880.
[48] Y. Huang, C. Powers, S.K. Madala, K.D. Greis, W.D. Haffey, J.A. Towbin, E. Purevjav, S. Javadov, A.W. Strauss, Z. Khuchua, Cardiac metabolic pathways affected in the mouse model of Barth syndrome, PLoS One 10 (2015) e0128561.
[49] K.M. Davies, T.B. Blum, W. Kuhlbrandt, Conserved in situ arrangement of complex I and III2 in mitochondrial respiratory chain supercomplexes of mammals, yeast, and plants, Proc. Natl. Acad. Sci. U. S. A. 115 (2018) 3024–3029.
[50] R. Guo, S. Zong, M. Wu, J. Gu, M. Yang, Architecture of human mitochondrial respiratory Megacomplex I2III2IV2, Cell 170 (2017) 1247–1257 (e1212).
[51] M. Wu, J. Gu, R. Guo, Y. Huang, M. Yang, Structure of mammalian respiratory supercomplex I1III2IV1, Cell 167 (2016) 1598–1609 (e1510).
[52] J.A. Letts, K. Fiedorczuk, L.A. Sazanov, The architecture of respiratory supercomplexes, Nature 537 (2016) 644–648.
[53] K.M. Davies, M. Strauss, B. Daum, J.H. Kief, H.D. Osiewacz, A. Rycovska, V. Zickermann, W. Kuhlbrandt, Macromolecular organization of ATP synthase and complex I in whole mitochondria, Proc. Natl. Acad. Sci. U. S. A. 108 (2011) 14121–14126.
[54] N. Pfanner, M. van der Laan, P. Amati, R.A. Capaldi, A.A. Caudy, A. Chacinska, M. Darshi, M. Deckers, S. Hoppins, T. Icho, S. Jakobs, J. Ji, V. Kozjak-Pavlovic, C. Meisinger, P.R. Odgren, S.K. Park, P. Rehling, A.S. Reichert, M.S. Sheikh, S.S. Taylor, N. Tsuchida, A.M. van der Bliek, I.J. van der Klei, J.S. Weissman, B. Westermann, J. Zha, W. Neupert, J. Nunnari, Uniform nomenclature for the mitochondrial contact site and cristae organizing system, J. Cell Biol. 204 (2014) 1083–1086.
[55] R. Richter-Dennerlein, A. Korwitz, M. Haag, T. Tatsuta, S. Dargazanli, M. Baker, T. Decker, T. Lamkemeyer, E.I. Rugarli, T. Langer, DNAJC19, a mitochondrial co-chaperone associated with cardiomyopathy, forms a complex with prohibitins to regulate cardiolipin remodeling, Cell Metab. 20 (2014) 158–171.
[56] V. Betaneli, E.P. Petrov, P. Schwille, The role of lipids in VDAC oligomerization, Biophys. J. 102 (2012) 523–531.